Supporting Information.

In-situ Atomically Dispersed Fe Doped Metal-Organic Framework on Reduced Graphene Oxide as Bifunctional Electrocatalyst for Zn-Air Batteries

Xiaolin Zhao[a,b,c,d]†*, Lin Shao[a,f]†, Ziming Wang[d], Huibing Chen[a,f], Haipeng Yang[e*] and Lin Zeng[a,f*]

[a] Department of Mechanical and Energy Engineering, Southern University of Science and Technology, Shenzhen 518055, China

[b] Shenzhen Automotive Research Institute, Beijing Institute of Technology, Shenzhen 518118, Guangdong, China

[c] National Engineering Laboratory for Electric Vehicles, Beijing Institute of Technology, Beijing 100081, Beijing, China

[d] Department of Chemical and Biological Engineering, University at Buffalo, The State University of New York, Buffalo, New York 14260, United States

[e] College of Materials Science and Engineering, Shenzhen Key Laboratory of Polymer Science and Technology, Shenzhen University, Shenzhen, 518060, China

[f] Guangdong Provincial Key Laboratory of Energy Materials for Electric Power, Southern University of Science and Technology, Shenzhen 518055, China

†**These authors contributed equally:** Xiaolin Zhao, Lin Shao

*** Corresponding Authors:**

E-mail addresses:

zhaoxiaolin@szari.ac.cn, yanghp@szu.edu.cn, zengl3@sustech.edu.cn

Figures S1 to S6;

Table S1-S6

2.Experimental Section

Catalysts synthesis

Graphene oxide (GO) synthesis

GO was prepared from natural graphite powder by using a modified Hummers' method.[1-4] Firstly, graphite powder (2 g) and $NaNO_3$ (1 g) were mixed with concentrated H_2SO_4 (46 mL) in an ice bath for 15-20 min. $KMnO_4$ (6 g) was added gradually under vigorous stirring to prevent rapid reaction temperature rise, which was kept the temperature lower than 20°C. The ice bathe was removed, and the mixture was stirred at 35°C for 2 h. At the end, deionized water (92 mL) was slowly added to the mixture, while maintaining stirring at 98°C for 15 min. Then, the deionized water (280 mL) and H_2O_2 (10 mL) were added to the solution, and the color turned yellow. The mixture was left overnight. The mixture was washed by 5% HCl and the deionized water for many times, up to the PH=7. As-prepared GO was further dispersed by ultrasonication treatment for 1 h , and finally the GO was obtained by freeze drying (-45°C) for 48 h.

Reduced graphene oxide (rGO) synthesis

The synthesized graphite oxide (0.2 g)[5, 6] was dispersed into deionized water by

sonication for 1 h to obtain the uniform brown-yellow graphene oxide solution (2 mg/ml).The pH of the solution was adjusted to 8.5 by slowly adding $NH_3 \cdot H_2O$. Then, hydrazine hydrate (2 ml) was adding into the solution for 4 h at 80℃. The suspension was filtered, and washed with ultrapure water and methanol. The rGO was obtained by drying in oven at 30°C for 24 h.

Fe-ZIF-8/rGO catalyst synthesis

The rGO powder was first dispersed into methanol (75mL) by sonication for 30 min. 24 mmol 2-methylimidazole was dissolved in other methanol (75mL). Then, 5.5 mmol $Zn(NO_3)_2 \cdot 6H_2O$ and 0.1 mmol $Fe(NO_3)_3 \cdot 9H_2O$ were adding into the rGO solution with vigorous agitation. After 30min, the 2-methylimidazole solution was adding into the above mixture with stirring for 30min. At last, the solution was heated at 60℃ for 24 h.The precipitant was collected by centrifugation and washed with ethanol at least three times. After drying at 60℃ in a vacuum oven, Fe-ZIF-8/rGO precursor was prepared, and denoted as Fe-ZIF-8/nrGO (n was weight ratio (rGO: Fe-ZIF-8), which were 1, 2, 3, 4). The pure Fe-ZIF-8 was synthesized by the same process, just no adding rGO. The different sizes of Fe-ZIF-8 particle were prepared by previous reports.[7, 8] The precursor was calcined at temperature range from 800 to 1100 ℃ under N_2 flow for 1 h. After carbonization, the catalysts were named as Fe-N-C/nrGO.

Physical characterization:

The surface morphology and microstructure of the samples were investigated with

scanning electron microscopy (SEM, Model JSM-6510A, Japan). Transmission electron microscopy (TEM) was performed on a JEOL JEM-2100 high-resolution transmission electron microscopes at 200 kV. The crystal phases present in each sample were identified using powder X-ray diffraction (XRD) on a Rigaku Ultima IV diffractometer with Cu K-α X-rays. X-ray photoelectron spectroscopy (XPS) was performed by using a Microlab 350 (Thermo Fisher Scientific). The N_2 adsorption/desorption isothermal was recorded on Micromeritics ASAP 2020. Raman spectroscopy was performed by Raman Microscope with a 532 nm excitation laser. Inductively coupled plasma (ICP) spectroscopy was conducted on a Dual-view Optima 5300 DV ICP-OEM system.The high angle annular dark-field scanning TEM (HAADF-STEM) were performed on a probe-corrected FEI Titan 80-300 S/TEM.

Electrochemical measurements:

The electrochemical measurements were measured by an electrochemical workstation (CHI760e) in a three-electrode cell for oxygen reduction reaction (ORR)/oxygen evolution reaction (OER) tests. A graphite rod as the counter electrode, a rotating-ring disc electrode as the working electrode, a reversible hydrogen electrode (RHE) was as the reference electrode. Each catalyst was mixed with isopropanol and a 5wt% Nafion solution to produce an ink.The catalyst loading of the samples was ~ 255 μg cm^{-2}. For comparison, the commercial Pt/C catalyst (20 wt %) was also prepared with a loading mass of ~ 30μg_{Pt} cm^{-2}.The loading amount of the IrO_2 on RDE was determined to be 0.2 mg/cm^2.

All the cyclic voltammetry (CV), ORR polarization curves and four-electron selectivity were recorded in N_2 or O_2- saturated 0.1M KOH at 50 mV s^{-1} for 30 cycles.

For ORR measurement: The linear sweeping voltammetry (LSV) was conducted at various rotation rates from 500 to 2500 rpm with a sweep rate of 5 $mV \cdot s^{-1}$ in O_2 or N_2-saturated 0.1 M KOH solution. The ORR current was calculated by deduction of the background capacitive current measured in Ar-saturated 0.1 M KOH solution.

The electron transfer number (n) of ORR is calculated by the K-L equation as follows [9]:

$$1/J = 1/J_k + 1/J_L = 1/J_k + 1/(B\omega^{1/2})$$

$$B = 0.2nFD^{2/3}v^{-1/6}C$$

$$J_k = nFkC$$

where J is the measured current density, J_L and J_k are the diffusion-limiting current density and the kinetic current density, where n is the electron transferred number, F is the Faraday constant(96500 $C \cdot mol^{-1}$), ω is the angular velocity (rpm), D is the diffusion coefficient of O_2 in 0.1 M KOH (1.9×10^{-5} $cm^2 \cdot s^{-1}$), C is the saturated concentration of O_2 in 0.1 M KOH at room temperature ($1.2\times10^{-6} mol \cdot cm^{-3}$),$v$ is the viscosity of the electrolyte ($0.01 cm^2 \cdot s^{-1}$), and k is the electron transfer rate constant.

For OER measurements: The LSV curves were performed by using RDE in 0.1 M KOH or 1M KOH at a scan rate of 5 mV s^{-1} under 1600rpm. The electrochemical active surface area of the samples was obtained by the double-layer capacitance (Cdl)

using the CV method in non-Faradaic window. The CV curves were obtained at scan rate of 5, 10, 15, 20, 25, and 30 mV s^{-1}.

Tafel slopes were obtained by fitting the linear regions of Tafel plots to the Tafel equation ($\eta = b \log |j| + a$, where b is the Tafel slope, j is the current density).

The durability test was carried out at a static overpotential for 10 h, during which the current variation with time was recorded.

Zn-air Battery assembly: The Zn-air battery tests were performed with a homemade Zn-air cell. The catalyst with a loading of 1.0 mg cm^{-2} was coated on a porous carbon paper was coated on a porous carbon paper (with a geometric area of 1 cm^2). A polished zinc plate was used as the anode. The waterproof and breathable membrane was used as the gas diffusion layer. 6 M KOH + 0.2 M $Zn(CH_3COO)_2$ solution was used as the electrolyte. The polarization curves were recorded by linear sweep voltammetry with a sweep rate of 10 mV s^{-1}. All Zn-air batteries were tested under the same experimental conditions.

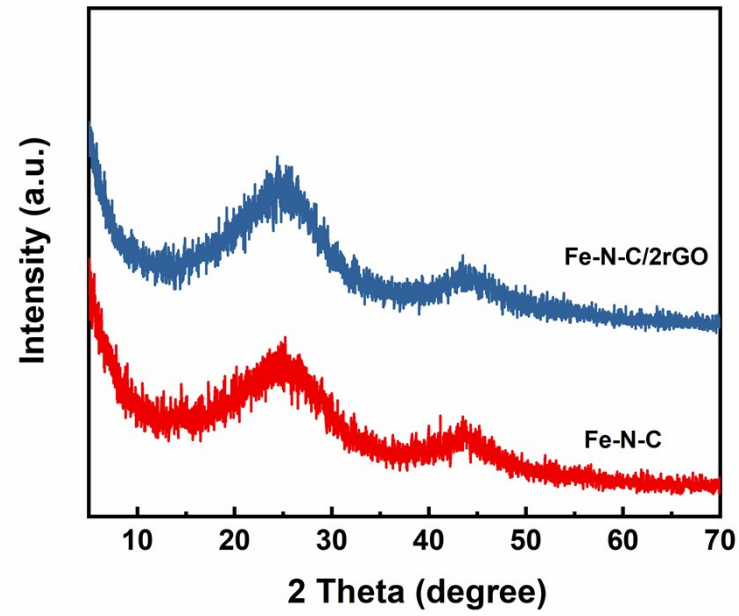

Figure S1. XRD patterns for the catalysts obtained after single heat-treatment at 1100 °C .

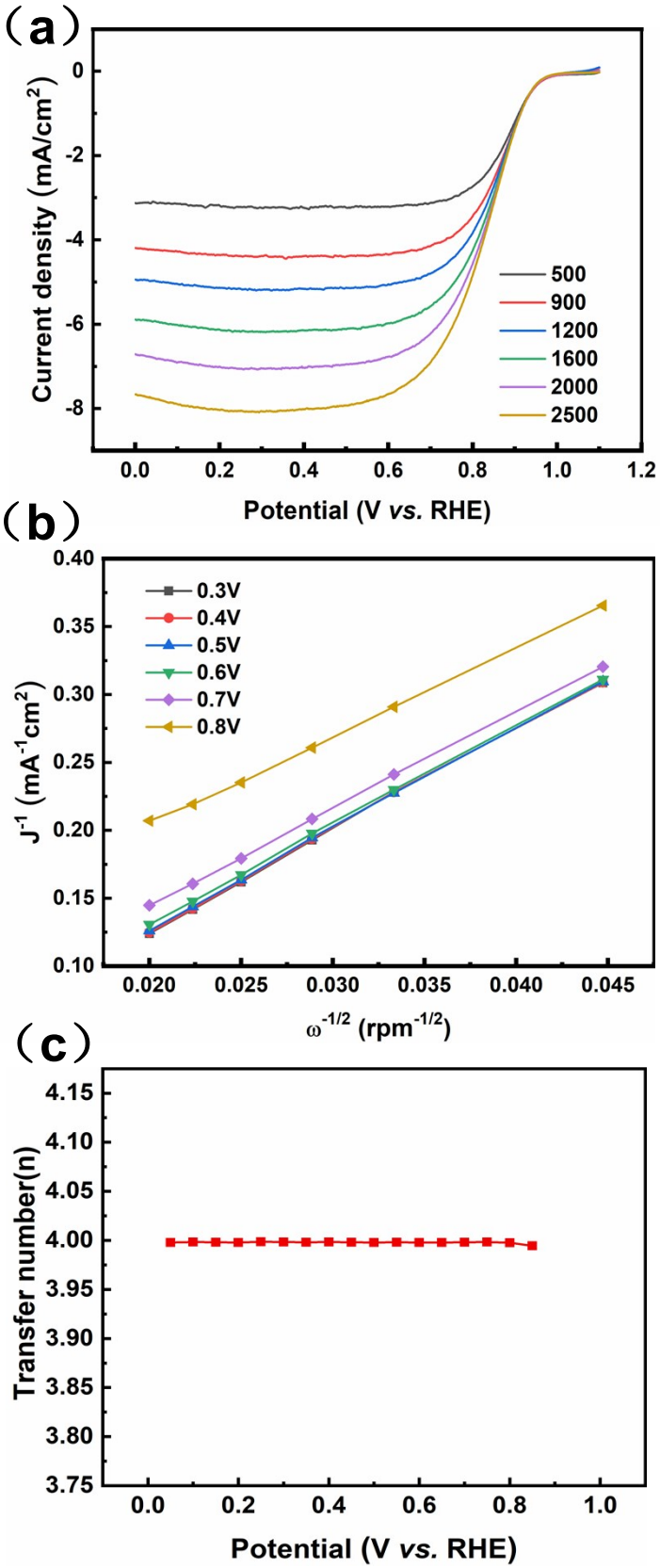

Figure S2. (a)The ORR kinetics of the Fe-N-C/2rGO catalyst were further analyzed by rotating disk measurement; (b)The corresponding Koutecky-Levich plots at different potentials; (c)The electron transfer number

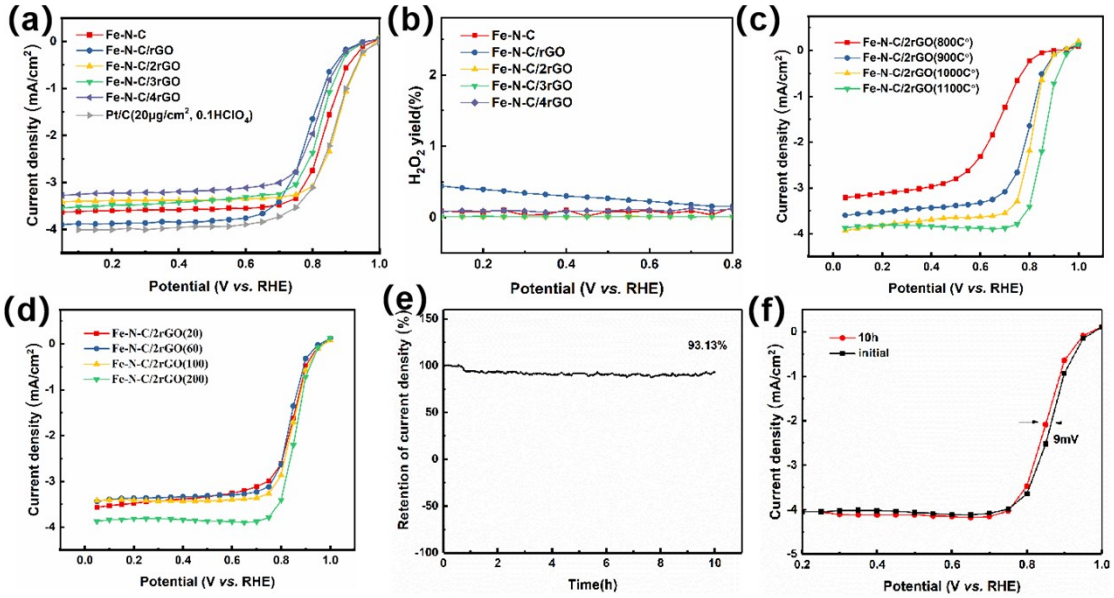

Figure S3. (a) ORR polarization plots and (b) H_2O_2% of all the catalysts; (c) ORR polarization plots of the catalysts synthesized at various temperatures; (d) the in-situ different sizes of the Fe-N-C catalysts; (e) 10h chronoamperometry tests at constant potentials of 0.85V; (f) ORR polarization plots after 10h. Test conditions: O_2-saturated 0.5 M H_2SO_4, 900 rpm, 25℃, catalyst loading of 0.6 mg cm^{-2}.

The hydrogen peroxide yield was calculated from the recorded ring (I_r) and disk current (I_d) using the following equation where N =0.36 is collection efficiency H_2O_2 yield (%) $=200I_r/(I_r+NI_d)$

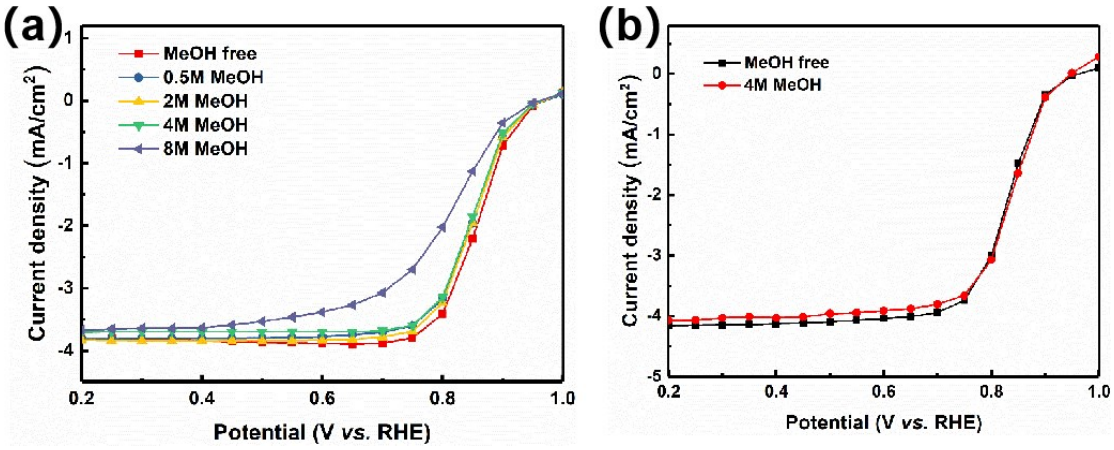

Figure S4. ORR polarization plots of the Fe-N-C/2rGO catalyst in O_2-saturated 0.5 M H_2SO_4 aqueous solution with a rotating rate of 900 rpm (a) containing different methanol concentrations (b) only 4M methanol concentration

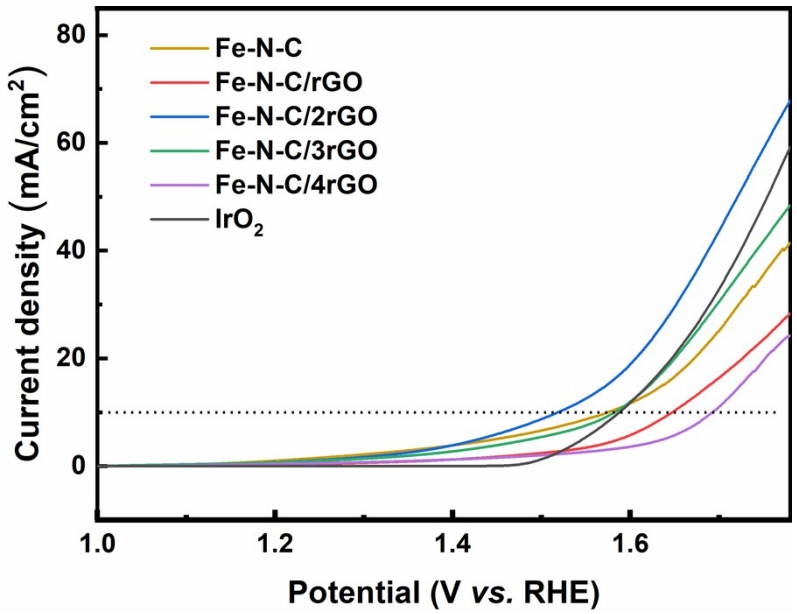

Figure S5.The OER polarization curves of all the catalysts;Test conditions: O_2-saturated 0.1 M KOH, 1600 rpm, 25℃, catalyst loading of 0.255mg cm^{-2}

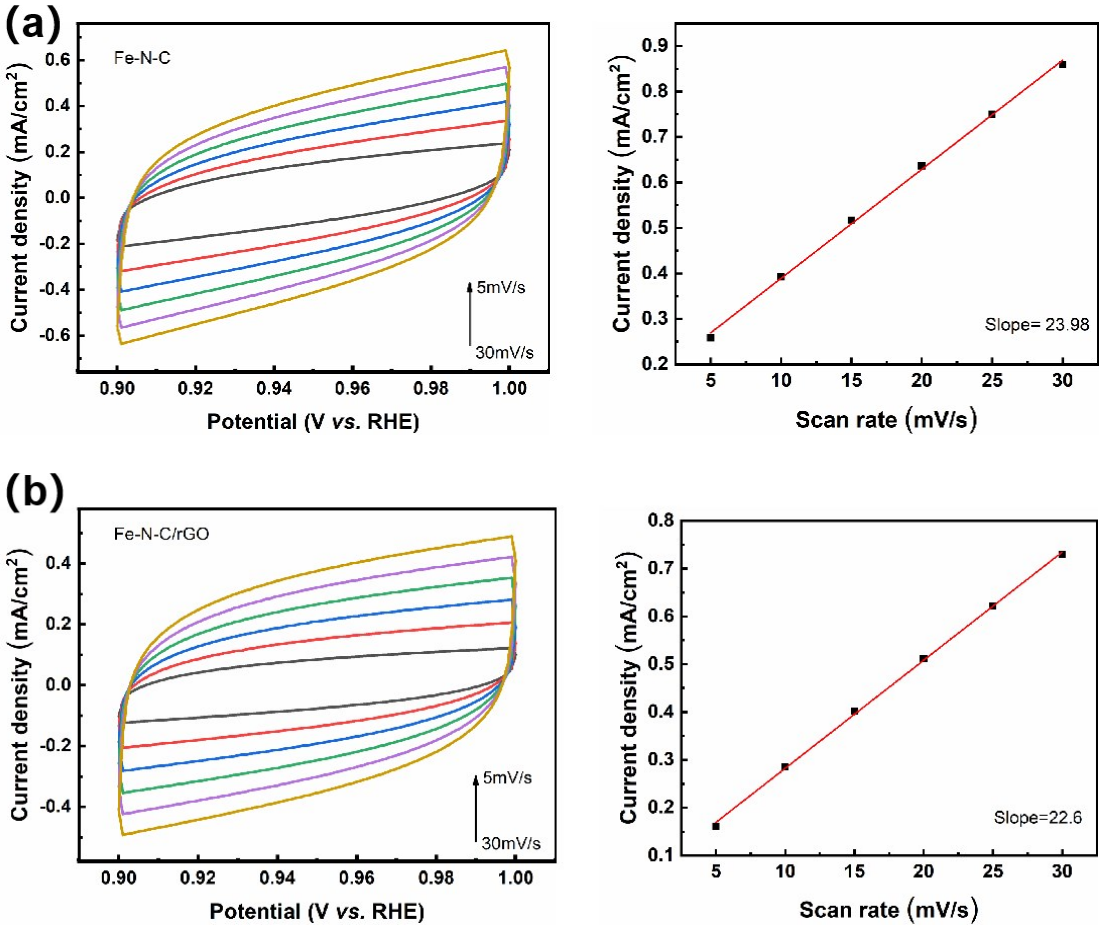
(a)
Fe-N-C
Current density (mA/cm^2)
Potential (V vs. RHE)
5mV/s
30mV/s
Current density (mA/cm^2)
Scan rate (mV/s)
Slope= 23.98
(b)
Fe-N-C/rGO
Current density (mA/cm^2)
Potential (V vs. RHE)
5mV/s
30mV/s
Current density (mA/cm^2)
Scan rate (mV/s)
Slope=22.6

(c)

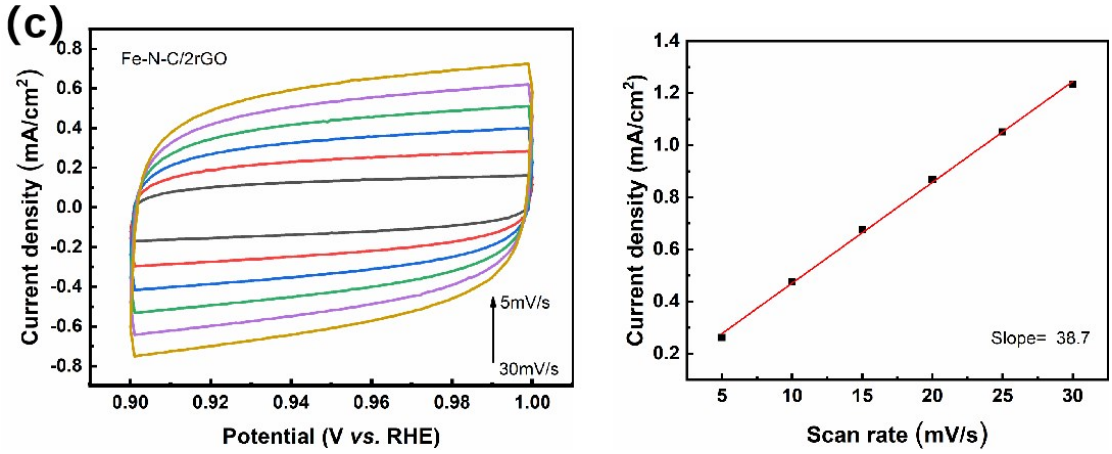
Fe-N-C/2rGO
Current density (mA/cm^2)
Potential (V vs. RHE)
5mV/s
30mV/s
Current density (mA/cm^2)
Scan rate (mV/s)
Slope= 38.7

(d)

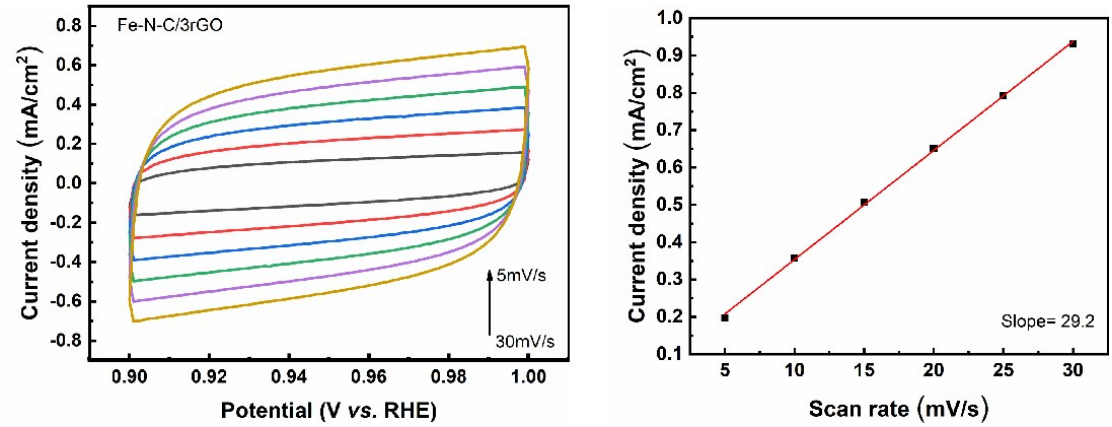
Fe-N-C/3rGO
Current density (mA/cm^2)
Potential (V vs. RHE)
5mV/s
30mV/s
Current density (mA/cm^2)
Scan rate (mV/s)
Slope= 29.2

(e)

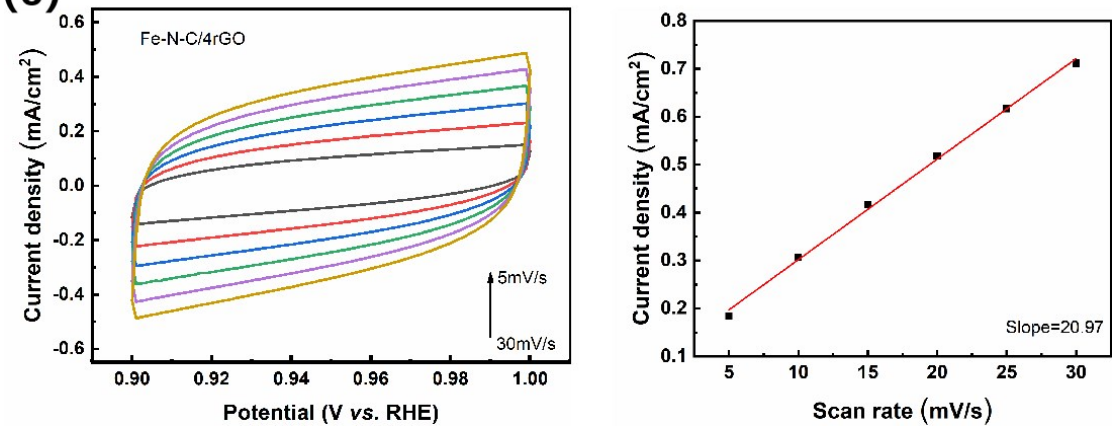
Fe-N-C/4rGO
Current density (mA/cm^2)
Potential (V vs. RHE)
5mV/s
30mV/s
Current density (mA/cm^2)
Scan rate (mV/s)
Slope=20.97

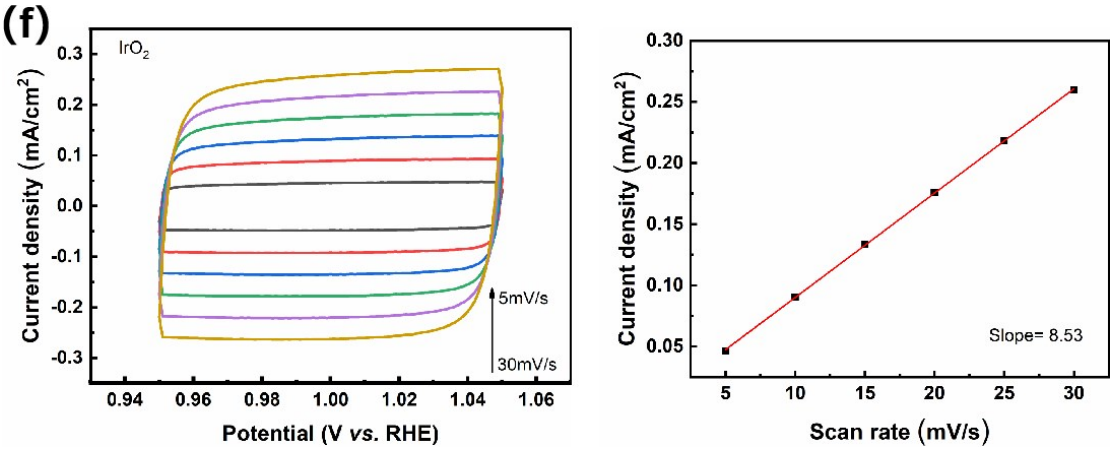

Figure S6. CV curves and the charging current density differences plotted against scan rates of (a) Fe-N-C, (b)Fe-N-C/rGO, (c) Fe-N-C/2rGO, (d)Fe-N-C/3rGO, (e)Fe-N-C/4rGO and (f) IrO_2 at various scan rates (5, 10, 15, 20, 25, and 30 mV s^{-1}).

Calculation of ECAS: The calculation of electrochemically active surface area (ECAS) is estimated from the double layer capacitance (C_{dl}) of the different catalysts in 1 M KOH based on the previous published report. The charging current (ic) was measured from the CVs at different scan rates. The relation between ic, the scan rate (ν) and the C_{dl} was given in equation (1): $ic = \nu C_{dl}$.

Therefore, the slope of ic as a function of ν is equal to C_{dl}. For the calculation of ECAS, the specific capacitance (Cs) value is 0.040 mF cm^{-2} in 1 M KOH. So the ECAS of is calculated according to equation (2): $ECSA=C_{dl}/Cs$.

The selected potential range was in non-Faradaic window.

Table S1. BET surface areas and Pore volume of the catalysts

Samples	V_{micro}		V_{meso}		V_{macro}		V_{total}	S_{BET}
	cm^3/g	%	cm^3/g	%	cm^3/g	%	cm^3/g	m^2/g
rGO	0.15	57.69	0.05	19.23	0.06	23.07	0.26	242
Fe-N-C/2rGO	0.37	46.84	0.32	40.51	0.10	12.65	0.79	571
Fe-N-C	0.30	53.57	0.02	3.77	0.21	39.62	0.53	445

Table S2. Elemental quantification determined by XPS for different catalysts (at%).

Samples	C	N	O	Fe	Zn
GO	73.17	--	26.83	--	--
rGO	92.94	--	7.96	--	--
Fe-N-C/2rGO	93.59	3.18	2.7	0.38	0.15
Fe-N-C	94.96	2.48	2.1	0.32	0.14

Table S3. The N1s spectra fitting results of catalysts of the Fe-N-C/2rGO and Fe-N-C(%).

Samples	**Pyridinic-N/Fe-N_X**	**Graphitic-N**	**Pyrrolinc-N**	**Oxidized graphitic-N**
Fe-N-C	25.73	35.88	21.38	17
Fe-N-C/2rGO	38.18	22.03	21.39	18.4

Table S4. The Fe2p spectra fitting results of catalysts of the Fe-N-C/2rGO and Fe-N-C(%).

Samples	**Fe2p3/2**	**Fe 2p1/2**
Fe-N-C/2rGO	65.10	34.90

Fe-N-C	60.87	39.13

Table S5. Elemental quantification of catalyst determined by ICP.

Samples	**Fe (wt%)**	**Zn (wt%)**
Fe-N-C/2rGO	0.45	0.63
Fe-N-C	0.43	0.71

Table S6. Summary of the catalytic activities of the reported composite electrocatalysts in 0.1 M KOH.

Catalyst	**E_{onset} (V vs RHE)**	**$E_{1/2}$ (V vs RHE)**	**I_K (mA cm^2) vs RHE**	**Ej=10 (V vs RHE)**	**ΔE （$E_{j=10}$-$E_{1/2}$） (V vs RHE)**	**Battery performancem （mW cm^{-2}）**	**Ref.**
Fe-N-C/2rGO	0.99	0.88		1.56	0.68	164	This work
FeP/Fe_2O_3@NPCA	0.95	0.838	5.357	1.632	0.794	——	[9]
Co–N_x/C NRA	——	0.877	——	1.53	0.65	193.2	[10]
Co@N-CNT/rGO-0.1	——	0.82	——	1.69	0.87	122	[11]
$Co_{5.47}$N@N-rGO-750	——	0.81	——	1.58	0.77	120.7	[12]
Co_3Fe_7@Fe_2N/rGO	0.98	0.89	——	1.6	0.71	——	[13]

C-MOF-C2-900	——	0.817	——	1.58 V	0.763	——	[14]
Fe/N-G-SAC	——	0.89	——	1.67	0.78	120	[15]
Fe-Nx-C	1.05	0.91	5.44	1.83	0.92	96.4	[16]
S,N-Fe/N/C-CNT	——	0.85	6.68	1.6	0.75	102.7	[17]
Fe-CN-CIG	——	0.84	5	1.67	0.83	——	[18]
FeCoNx-CN	0.954	0.886	6.3	1.67	0.784	150	[19]
$Fe_{0.5}Co_{0.5}$/NrGO	——	0.85	5.25	1.63	0.78	86	[20]
Fe-Nx-PNC	0.997	0.86	6	1.63	0.77	118	[21]

References:

[1] W.S. Hummers, R.E. Offeman, Journal of the American Chemical Society 80 (1958) 1339-1339.

[2] L. Han, X. Lu, M. Wang, D. Gan, W. Deng, K. Wang, L. Fang, K. Liu, C.W. Chan, Y. Tang, Small 13 (2017) 1601916.

[3] F. Luo, K. Wu, J. Shi, X. Du, X. Li, L. Yang, M. Lu, Journal of Materials Chemistry 5 (2017) 18542-18550.

[4] D.C. Marcano, D.V. Kosynkin, J.M. Berlin, A. Sinitskii, Z. Sun, A. Slesarev, L.B. Alemany, W. Lu, J.M. Tour, Acs Nano 4 (2010) 4806.

[5] D. Li, M.B. Muller, S. Gilje, R.B. Kaner, G.G. Wallace, Nature Nanotechnology 3 (2008) 101-105.

[6]S. M. Kang, S. Park, D. Kim, S. Y. Park, R. S. Ruoff, H. Lee, Advanced Functional Materials 21 (2011) 108-112.

[7] H. Zhang, S. Hwang, M. Wang, Z. Feng, S. Karakalos, L. Luo, Z. Qiao, X. Xie, C. Wang, D. Su, Journal of the American Chemical Society 139 (2017) 14143-14149.

[8] Y. He, S. Hwang, D.A. Cullen, M.A. Uddin, L. Langhorst, B. Li, S. Karakalos, A.J. Kropf, E.C. Wegener, J. Sokolowski, Energy & Environmental Science 12 (2019) 250-260.

[9] K. Wu, L. Zhang, Y. Yuan, L. Zhong, Z. Chen, X. Chi, H. Lu, Z. Chen, R. Zou, T. Li, C. Jiang, Y. Chen, X. Peng, J. Lu, Advanced Materials, 32 (2020)2002292.

[10] I.S. Amiinu, X. Liu, Z. Pu, WenqiangLi, S. Mu, Advanced Functional Materials 28 (2018) 1704638.

[11] X. Peng, L. Wei, Y. Liu, T. Cen, D. Yuan, Energy & Fuels 34 (2020).

[12] X.S. A, S.C. A, S.C. A, W.P. B, J.Z. A, Carbon 157 (2020) 234-243.

[13] D. Liang, H. Zhang, X. Ma, S. Liu, T. Huang, Materials Today Energy 17 (2020) 100433.

[14] M. Zhang, Q. Dai, H. Zheng, M. Chen, L. Dai, Advanced Materials 30 (2018) 1705431.

[15] M. Xiao, Z. Xing, Z. Jin, C. Liu, J. Ge, J. Zhu, Y. Wang, X. Zhao, Z. Chen, Advanced Materials 32 (2020) 2004900.

[16] J. Han, X. Meng, L. Lu, J. Bian, Z. Li, C. Sun, Advanced Functional Materials 29 (2019) 1808872.

[17] P. Chen, T. Zhou, L. Xing, K. Xu, Y. Tong, H. Xie, L. Zhang, W. Yan, W. Chu, C. Wu, Y. Xie, Angewandte Chemie International Edition 56 (2017) 1-6.

[18] D. P. He, Y. L. Xiong, J. L. Yang, X. Chen, Z. X. Deng, M. Pan, Y. D. Li, S. C. Mu, Journal of Materials Chemistry A 5(2017) 1930.

[19] S. Li, C. Cheng, X. J. Zhao, J. Schmidt, A. Thomas, Angewandte Chemie International Edition 57(2018) 1856.

[20] L. Wei, H.E. Karahan, S. Zhai, H. Liu, X. Chen, Z. Zhou, Y. Lei, Z. Liu, Y. Chen, Advanced Materials 29 (2017) 1701410.

[21] L. Ma, S. Chen, Z. Pei, Y. Huang, G. Liang, F. Mo, Q. Yang, J. Su, Y. Gao, J.A. Zapien, ACS Nano (2018) (2018) 1949.